INTERNATIONAL JOURNAL OF AUTOMOTIVE AND MECHANICAL ENGINEERING (IJAME)
ISSN: 2229-8649 e-ISSN: 2180-1606
VOL. 19, ISSUE 2, 9859 – 9871
DOI: https://doi.org/10.15282/ijame.19.2.2022.18.0760

ORIGINAL ARTICLE

Investigation of Single-stage and Two-stage Forming Limit Curve of Aluminum 6061 with Different Temperatures and Strain Rates

M. Shekarzadeh and E. Hosseini*

Department of Mechanical Engineering, Ahvaz Branch, Islamic Azad University, 61349-37333, Ahvaz, Iran

ABSTRACT – The Form Limit Curve (FLC) is an important and helpful concept for defining sheet metal ductility. The ductility of aluminum 6061 alloy sheet was analyzed in this work. The current study examined how to enhance the formation curve of aluminum 6061, which is frequently utilized in the automotive industry. These curves were plotted and compared at various temperatures and strain levels. Using the finite element approach, the formation curve of this alloy was produced under the impact of various temperatures and strain rates. The forming limit curve was accomplished in two-stage forming when the pre-stress was formed in the sheet, and this curve was predicted for different temperatures using the one-stage forming behavior pattern. It was determined that increasing the temperature led the curve to rise and fall, but increasing the strain rate caused the curve to fall and contract. It was also revealed that by using the curvature of the forming limit curve in single-stage forming at various temperatures and a two-stage forming limit curve at one temperature, it was feasible to estimate two-stage FLC at two temperatures.

ARTICLE HISTORY
Received: 19th Feb 2022
Revised: 6th June 2022
Accepted: 27th June 2022
Published: 5th Aug 2022

KEYWORDS
Aluminum 6061;
Forming limit curve;
Multi-step forming;
Finite element method

INTRODUCTION

Aluminum alloys with high strength are utilized to reduce vehicle weight. Aluminum 6061 is frequently used in the automotive industry for a variety of components. Deep drawing is an important and delicate manufacturing method used in the mass manufacture of automotive and aerospace parts [1]. The variables of this process that play a role in the success or failure of the forming are the radius of curvature of the punch and the matrix of their distance, punch speed, strain rate, temperature, and coefficient of friction [1-5]. With the hot forming of aluminum alloy, its ductility is greatly improved, and in hot forming, strain rate plays a substantial role in ductility of the sheet. Therefore, describing the ductility of aluminum, which is determined by the forming limit curve at high temperatures and different strain rates, is very important to control the success of the forming process [6]. This curve was first described by Killer & Bacoffen [7], and Goodwin [8] and later became an industrial method and also a research topic, both theoretically and practically. This curve shows the strain limit that the sheet metal can withstand as it forms. Nakajima and Marciniak [8-10] presented tests published in the international standard ISO12004-2 that extract the strain limit curve at ambient temperature and quasi-static loading, which can be generalized to higher temperatures and strain rates. Laboratory tests have shown that the mentioned parameters and influencing the forming process also affect the FLC. Naka et al. [11] experimentally evaluated the impacts of forming speed and temperature on the forming limit diagram (FLD) for a fine-grain Al–Mg alloy (5083-O) sheet by conducting stretch-forming experiments at two different types of speeds and temperatures. In the study of Graf and Hasford [12], the Marciniak and Kuczynski (M-K) analytical approach for determining the shape of forming limit diagrams (FLDs) using high-exponent yield criteria has been expanded to incorporate the impact of modifying the strain patterns and applied to aluminum alloy 2008 T4.

Simulations that include gradual strain-path variations, as seen when extending over a hemispherical dome, suggested that the FLD's minimum moves to the right. Matsuoka and Sudo [13] indicated that the forming curve for a biaxial pre-strain sheet is different from that without pre-strain. In a study done by Bandyopadhyay et al. [14], laboratory scale two-stage stretch forming procedures were developed and produced, in which an interstitial free (IF) steel was first pre-strained in biaxial tensile mode and then deformed in tension–tension and tension-compression modes in a limiting dome height (LDH) test procedure. In their study, experimental results were used to validate the expected thickness distribution, maximum thinning position, and load progression curve during the second stage LDH test. Moreover, the stress-based forming curve was estimated using the strain-based forming curve and the Hill [15] and Bunge et al. [16] theory and finite element analysis. In the research work of Hashemi et al. [17], seven distinct ductile failure criteria are employed in finite element simulations to derive the forming limit diagram (FLD) of Al6063 aluminum tubes at high temperatures. The analysis of temperature and strain rate revealed that rising temperature leads the forming limit to increase, whereas increasing strain rate causes it to drop. Rahmani et al. [18] examined the temperature effect on the formability of AA6063 aluminum tubes during the incremental forming process. The experiments were carried out using AA6063 aluminum tubes. The tube wall was gradually expanded by a spirally moving instrument. In their study, the expansion ratio increased from 28% to 34% as the temperature rised from 100°C to 300°C, according to the findings. Surface roughness and bulge diameter were best controlled by axial feeding and temperature, respectively. Saxena et al. [19] evaluated the performance

*CORRESPONDING AUTHOR | E. Hosseini | ✉ ebrahim.2019.hosseini@gmail.com

of stamping lubricants during elevated temperature forming of SS304 sheets using the forming limit diagram. Forming limit diagrams (FLD) were plotted, and lubricant performance was assessed. When compared to MoS_2, it has been proven that conventional lubricant and high temperature grease are more reliable at elevated temperatures. Li et al. [20] addressed the impacts of strain paths and microstructure development on the forming limit diagram using a forming limit test for an AZ31B alloy sheet under strain path variations. The development of dislocation density during annealing in the pre-strained FLD test at 200°C was studied, and pre-strained FLD predictions were significantly improved.

As a result, the temperature throughout the process and the varying strain rates during the forming of aluminum 6061 at varying temperatures would substantially involve the design of the forming process in the present research. This is also necessary while developing the forming process and choosing the right equipment. The FLC is a criterion for predicting sheet ductility, however, it is not applicable to complicated forming processes. The present study focused on ways of improving the formation curve of aluminum 6061, a popular material in the automotive industry. These curves were generated and compared at various temperatures and strain levels. The formation curve of this alloy was calculated using finite element analysis under the influence of different temperatures and strain rates.

METHODOLOGY

The finite element model was applied in ABAQUS software in order to model the aluminum 6061 sheet forming process. In the present model, a fixed matrix and a punch with vertical motion were considered and an analytical rigid was used. Aluminum sheets were modeled in three dimensions (3D) and ductility based on previous studies [6,7,21] with different widths to obtain the forming curve (Figure 1 and Table 1). The elastoplastic properties, yield strength, and temperature elongation coefficient of these sheets, which vary with temperature and strain rate, were introduced [22-30]. The assembled model for two samples of sheets with different widths is depicted in Figure 2. In different analyzes, the punch was moved at a variable speed to form an aluminum sheet to create a constant strain rate. In addition, diverse temperatures were applied to the aluminum sheet for this process (Table 2). The sheets were meshed and analyzed using standard 10-point quadratic pyramid elements. In the two-stage forming model, in the first stage, the punch with a greater radius of curvature created a pre-strain on the sheet, and then in the second stage, the main punch with a smaller radius of curvature created more deformation in the sheet [14,21,23]. The properties of the material and the type of element were considered the same as in the single-stage model. In this section, a two-stage model was analyzed at ambient temperature for different sheet widths. Then, after performing data analysis on the results, a two-stage model for several different widths and temperatures with similar conditions to previous analyzes was investigated.

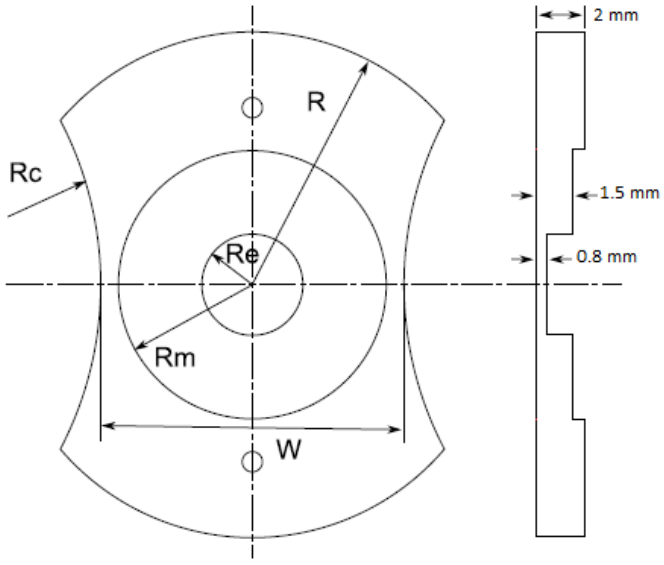

Figure 1. Sheet geometry.

Table 1. Dimensions of the modeled sheet in finite element analysis of forming.

Cases	1	2	3	4	5	
W (mm)	20	30	50	60	80	100
R (mm)			50			
Rc (mm)			70			
Re (mm)			10			

Table 2. Strain rate and temperature conditions in the finite element forming analysis.

Strain rate (1/s)	0.08, 0.8, 8	0.08, 0.8, 8	0.08, 0.8, 8	0.08, 0.8, 8
Temperature (°C)	24	140	200	400

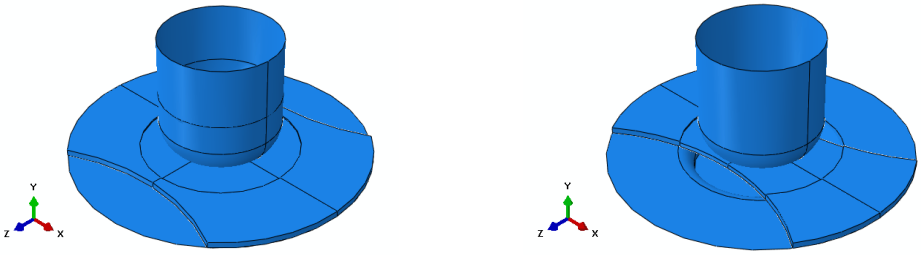

(a) (b)

Figure 2. Finite element model in ABAQUS software at (a) width: 60 and (b) width: 30.

VALIDATION

In the present research, the results of Zhang et al. [21] were adopted for validation. In the mentioned ref. [21], the Voce Hardening law was utilized to explain the theory of aluminum alloy behavior in forming. An approach was suggested in their work to evaluate the temperature and strain rate impacts on AA5086 formability by integrating a modified Voce constitutive model with the numerical simulation of the Marciniak test. The behavior of AA5086 alloy was considered by utilizing a modified model of this rule called Lin-Voce. In this case, stress was determined by yield strength, temperature, strain, and strain rate.

$$\bar{\sigma} = \sigma_Y + (C_1 + C_2 T)\sqrt{1 - exp(-C_3\bar{\epsilon})}\,\bar{\epsilon}^{C_4 \exp(C_5 T)} \quad (1)$$

where $\bar{\sigma}$ is the flow stress, σ_Y is the yield stress, C_1 and C_2 are the strain hardening coefficients, C_3 is the strain softening coefficient, C_4 and C_5 are strain rate sensitivity coefficients.

Since it is difficult to obtain the above relational constants, the inverse analysis method was used in the present work. By using laboratory data and numerical simulation by continuous iterations, these parameters were specified. Because the yield strength of aluminum was temperature-dependent and was based on the strain rate, according to ref. [21], the yield was applied as a function of temperature according to Table 3. The tensile test data in ref. [21] of the same group for diverse temperatures and forming rates were used for reverse analysis. By using the fitted curves on the force-time diagram, which is shown in Figure 3, the Lin-Voce relation constants are presented in Table 4.

Table 3. Yield strength for temperatures in AA5086 [21].

Temperature (°C)	Yield strength (MPa)
20	134.81
230	133.43
290	125.51

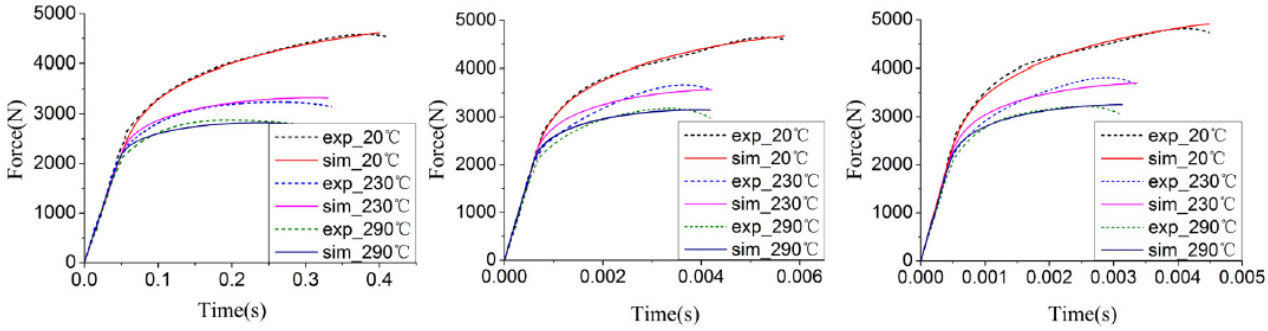

(a) (b) (c)

Figure 3. Comparison of the laboratory force-time fitted curves with Lin-Voce model for (a) 10 mm/s, (b) 750 mm/s and (c) 1000 mm/s.

Table 4. Lin-Voce relationship parameters using an inverse analysis method.

Tensile Speed	C_1	C_2	C_3	C_4	C_5	Deviation
10 mm/s	756.26	-1.0387	1.5508	0.00974	0.00003868	1.86%
750 mm/s	726.88	-0.8693	1.2932	0.00317	0.00003166	2.66%
1000 mm/s	698.83	-0.8392	1.5714	0.01038	0.00002545	2.48%

To validate this model, the Marciniak test was designed, as illustrated in Figure 4. By using a correlation of digital images with the camera during the testing process, the strain limit of each sample was obtained. Different strain paths for a uniaxial strain to plane strain and equal biaxial strain were covered using 13 specimens (Figure 5). Samples were

designed with non-uniform thickness to ensure maximum deformation occurs in the middle region of the sheet. Finally, the test was performed at a punch speed of 10 mm/s at room temperature. A throat-shaped occurrence appeared in concentrated regions when the average plastic strain ratio in concentrated and decentralized areas reached 7. At this point, the main stress in the concentrated region remained in the form of limit strain.

Finally, the Marciniak test is carried out under a punch speed of 10 mm/s at room temperature. To predict the occurrence of necking, a failure criterion widely used for the Marciniak-Kuczynski model is adopted: when the ratio of average equivalent plastic strain increments in the localized and non-localized zone reaches 7, localized necking is assumed to occur. At this moment, the principal strains in the localized zone are retained as limit strains.

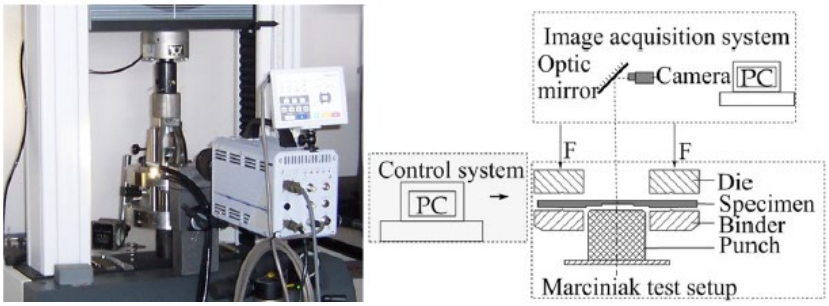

Figure 4. Marciniak test.

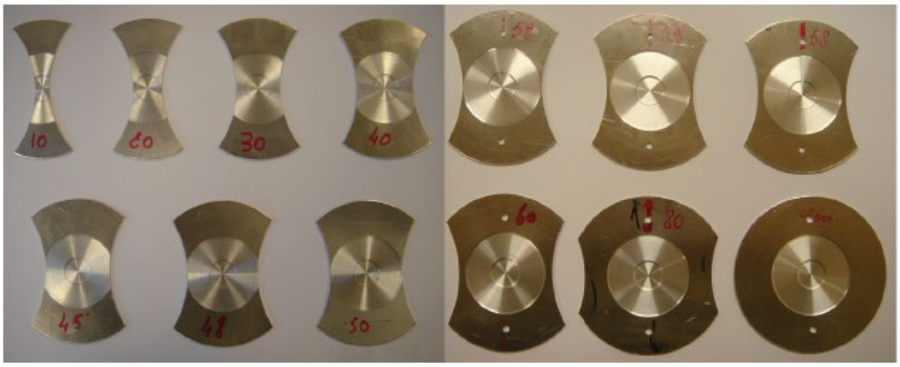

Figure 5. Considered samples in the test.

Based on laboratory tests, the finite element model consisted of three parts—a rigid cylindrical pan with a flat bottom, a rigid matrix, and a malleable specimen. Given a quarter symmetry in geometry and boundary conditions, only a quarter of the components were modeled (Figure 6). The matrix was tightened during the process and the punch moved downwards with vertical force. A compressive force of 100 KN was imposed on the surface of the specimen to prevent it from slipping on the matrix. Because of the non-uniform thickness of the sample, the center of the sample with a thickness of 0.8 mm and the pan did not come into contact in the test. The friction coefficient between this part of the sample and the punch was considered to be 0, the end of this coefficient between the punch and the 1.5 and 2 mm thicknesses of the sample was assumed to be 0.05 and 0.1, respectively. The finite element model was simulated and analyzed using the ABAQUS software.

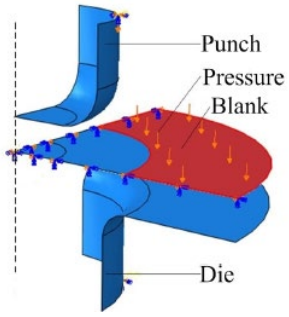

Figure 6. Finite element model of the present research.

The properties used for aluminum alloy were calculated and applied with the constants presented in ref. [21] and the Lin-Voce relation for the temperature and strain rate adopted in the present analysis. The matrix was tightened during the process and the punch moved downwards at a speed of 10 mm/s. Furthermore, to prevent the sheet from slipping on the matrix, a force of 100 KN is similar to the mentioned ref. [21] applied to the sheet. The aluminum sheet was meshed using quadratic elements of 10 nodes and for each of the 7 models, the ductility analysis of aluminum was performed. The predicted results were compared with the results presented in ref. [21] which is depicted in Figure 7. As it can be

seen in Figure 7, excellent agreement was achieved between the extracted results and the results of ref. [21], which can be concluded that the present finite element model is correct and has high accuracy. The first point on the left side of the graph was the aluminum sheet with W20, and therefore; by moving to the right of the graph, the value of W increased, and at the last point on the right side of the graph, it reached 100.

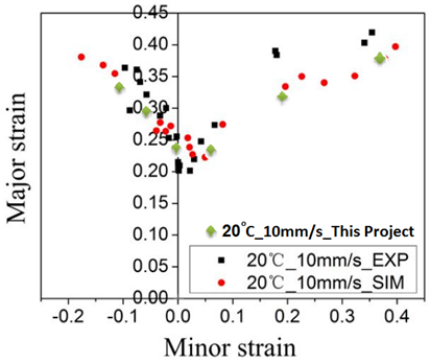

Figure 7. Comparison of present results (green points) with the results of ref. [21] (red points: numerical modeling, black points: test results.

Figure 8 and Figure 9 depict the results obtained from these simulations and graphs fitted to the results. It can be seen from Figure 8, the forming temperature had a remarkable impact on the curvature of forming limit. The strain increased by raising the temperature at a punch rate of 10 mm/s. Compared to the ambient temperature, the limit strain in a uniaxial tensile test, plate strain, and biaxial strain raised by 51.3%, 92.9%, and 116.59%, respectively. Nevertheless, during dynamic forming circumstances, at velocities of 750 and 1000 mm/s, the impact of strain rate was reversed, and ductility at 200°C was lower than at 20°C. Furthermore, when the temperature increased, the positive effect of rising temperature eventually compensated for the negative impact of strain rate, and the ductility curve approximated 20°C at 300°C. In Figure 9, the ductility curve at high punch speeds was always lower than the same curve at low speeds at the same temperature. For example, at 200°C, compared to 20°C, at 1000 mm/s, uniaxial strain, plate strain, and biaxial strain decreased by 36.1%, 45.2%, and 50.2%, respectively.

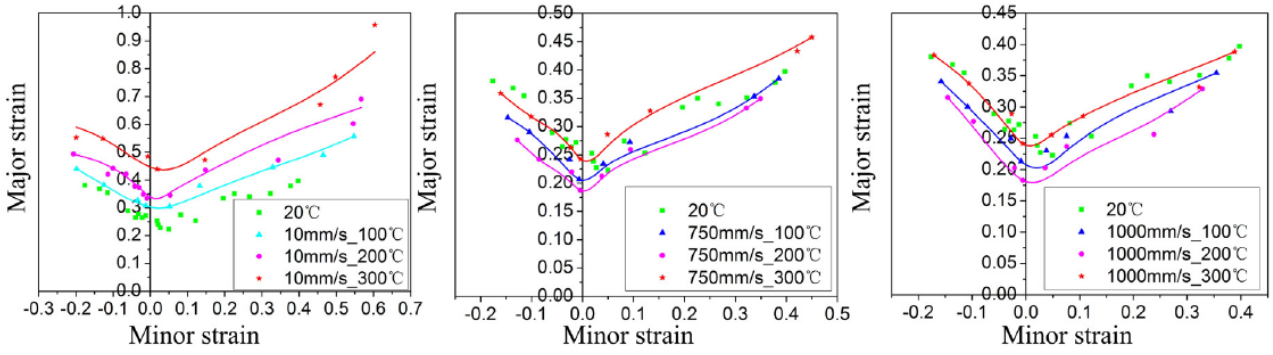

Figure 8. Comparison of the FLC for various temperatures at a given punch speed for (a) 10 mm/s, (b) 750 mm/s and (c) 1000 mm/s.

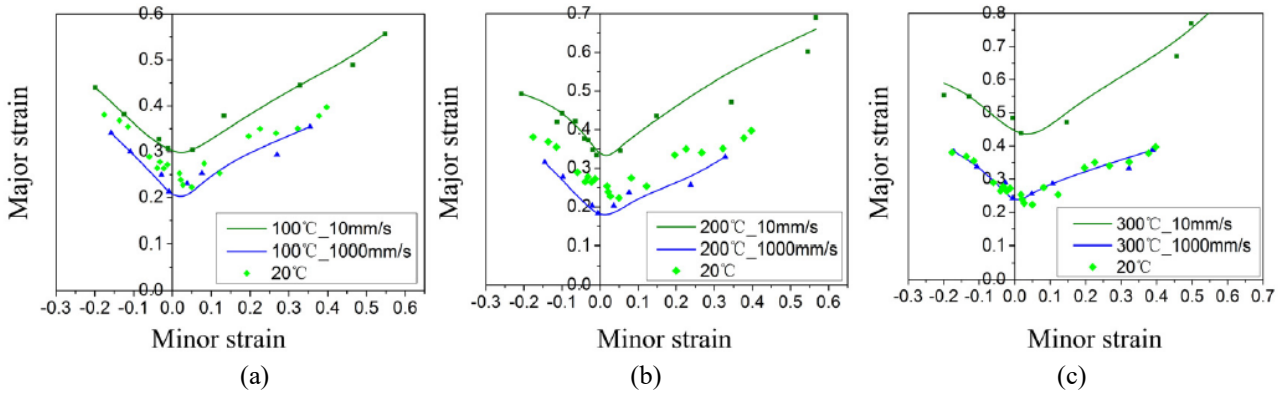

Figure 9. Comparison of the FLC under various pan speeds at (a) 100°C, (b) 200°C and (c) 300°C.

Hence, temperature and strain rate were effective in the hot ductility of aluminum alloys. At low forming speeds, temperature plays a major role. At high forming speeds, on the other hand, the negative influence of strain rate was

underlined, and the sheet was less ductile. The favorable effect of temperature increased and offset the negative effect of strain rate as the temperature grew. When the temperature reached 300°C, a balance was established between the impacts of temperature and the amount of strain, and the ductility of the sheet was close to room temperature at this degree. Six models were created under various strain situations in order to verify the current model. These models, like the first section of this study, were tested at a punching speed of 10 mm/s at a temperature of 20°C. Figure 10 depicts the models developed in the ABAQUS software. In all of these models, non-uniformly thick aluminum sheets were modeled as in ref. [21].

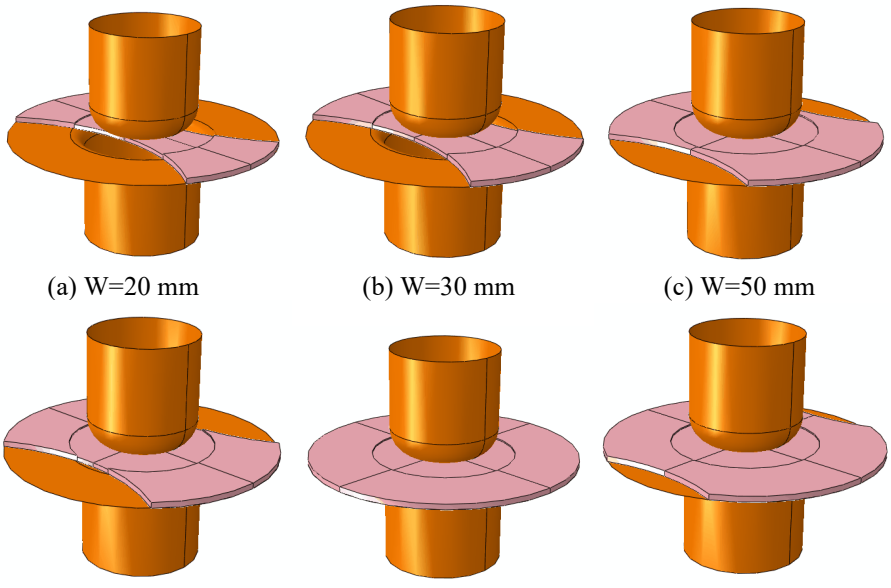

(a) W=20 mm (b) W=30 mm (c) W=50 mm

(d) W=60 mm (e) W=80 mm (f) W=100 mm

Figure 10. Prepared models for different strain conditions.

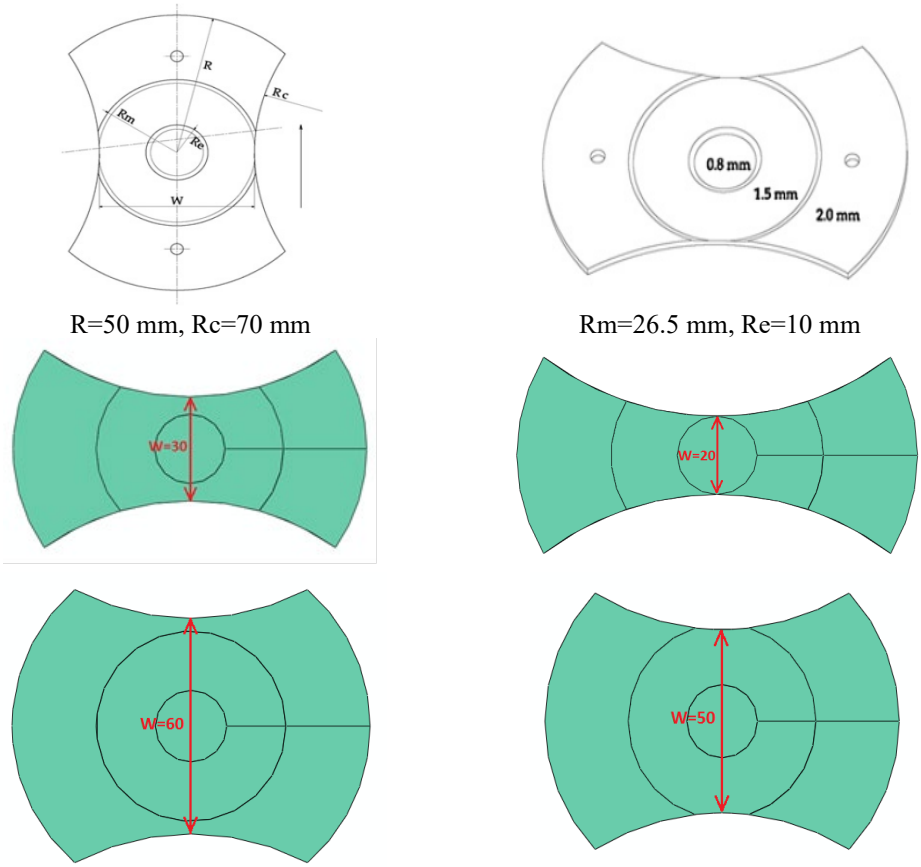

R=50 mm, Rc=70 mm Rm=26.5 mm, Re=10 mm

Figure 11. Model of aluminum sheets.

To achieve different strain conditions, the W parameter was considered as 20, 30, 50, 60, 80, and 100 for six models (Figure 11). By varying the specimen width, the lateral constraint can be varied to achieve failure in modes ranging from

uniaxial tension through-plane strain to balanced biaxial tension. The strain rate is also changed and fracture limits in other strain modes than plane strain may be determined. To fully understand the process, Figure 12 indicates the distribution of Von-Mises stress with actual deformation in aluminum sheets.

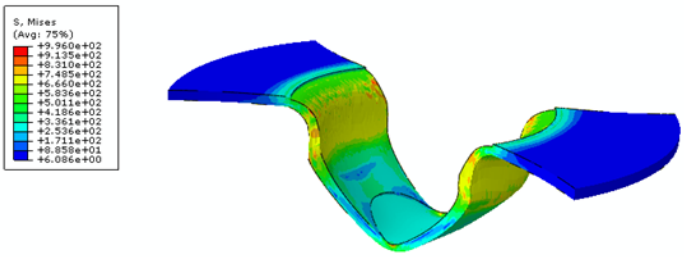

(a) W=20 mm

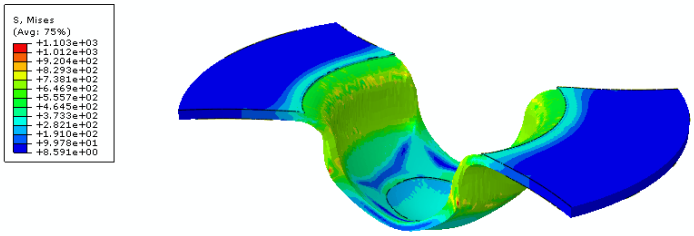

(b) W=30 mm

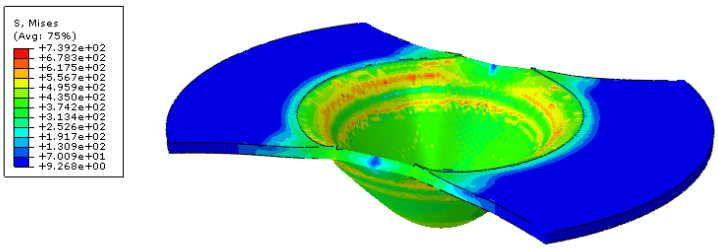

(c) W=50 mm

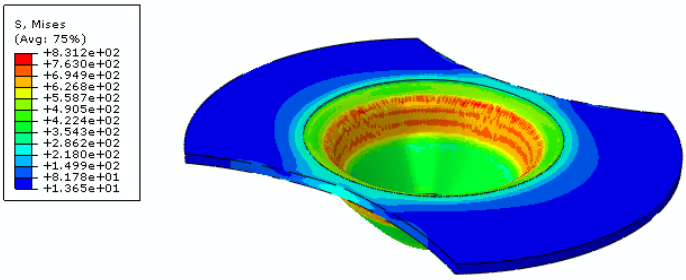

(d) W=60 mm

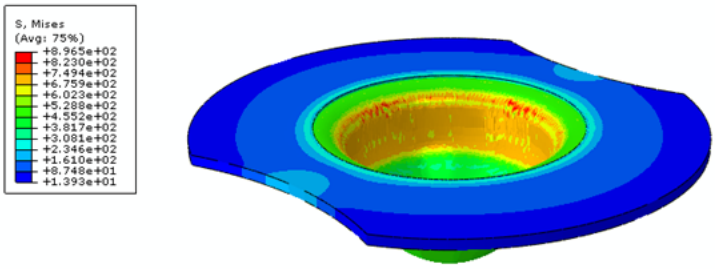

(e) W=80 mm

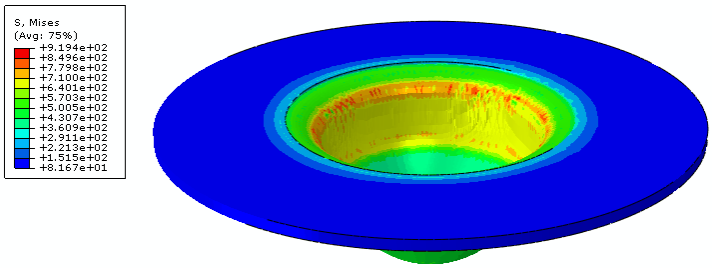

(f) W=100 mm

Figure 12. Von Mises stress distribution in aluminum sheets.

RESULTS AND DISCUSSION

By extracting the calculated strains at the end of the forming process, the FLC was obtained. The points in Figures 13 to 16 are related to different widths from left to right (20, 30, 50, 60, 80 and 100 mm). In short sheet width, the major strain had a positive value and the minor strain had a negative value. As the width of the sheet increased, the positive value of the major strain decreased, and the negative value of the minor strain was reduced. Within 50 mm, the value of the minor strain was almost zero and the strain of the major was at its lowest. As the width of the sheet raised, the strain of the major began to increase, and the strain of the minor moved from zero to positive values. In Figure 13, the forming limit curve for the analyzed temperatures at the three constant strain rates in the aluminum alloy sheet was compared. As the temperature increased, the curvature of the forming limit moved upwards and also became slightly more elongated. For temperatures of 140°C and 200°C, the curves obtained close to each other, but for the temperatures of 24°C and 400°C, there was a greater difference. Figure 14 demonstrates the forming limit curve to observe the impact of strain rate of the forming process at various temperatures. As the strain rate raised, the strain values decreased and the forming limit curve jumped down and became slightly more compact. For the analyzed strain rates, changes less than the analyzed temperatures were observed.

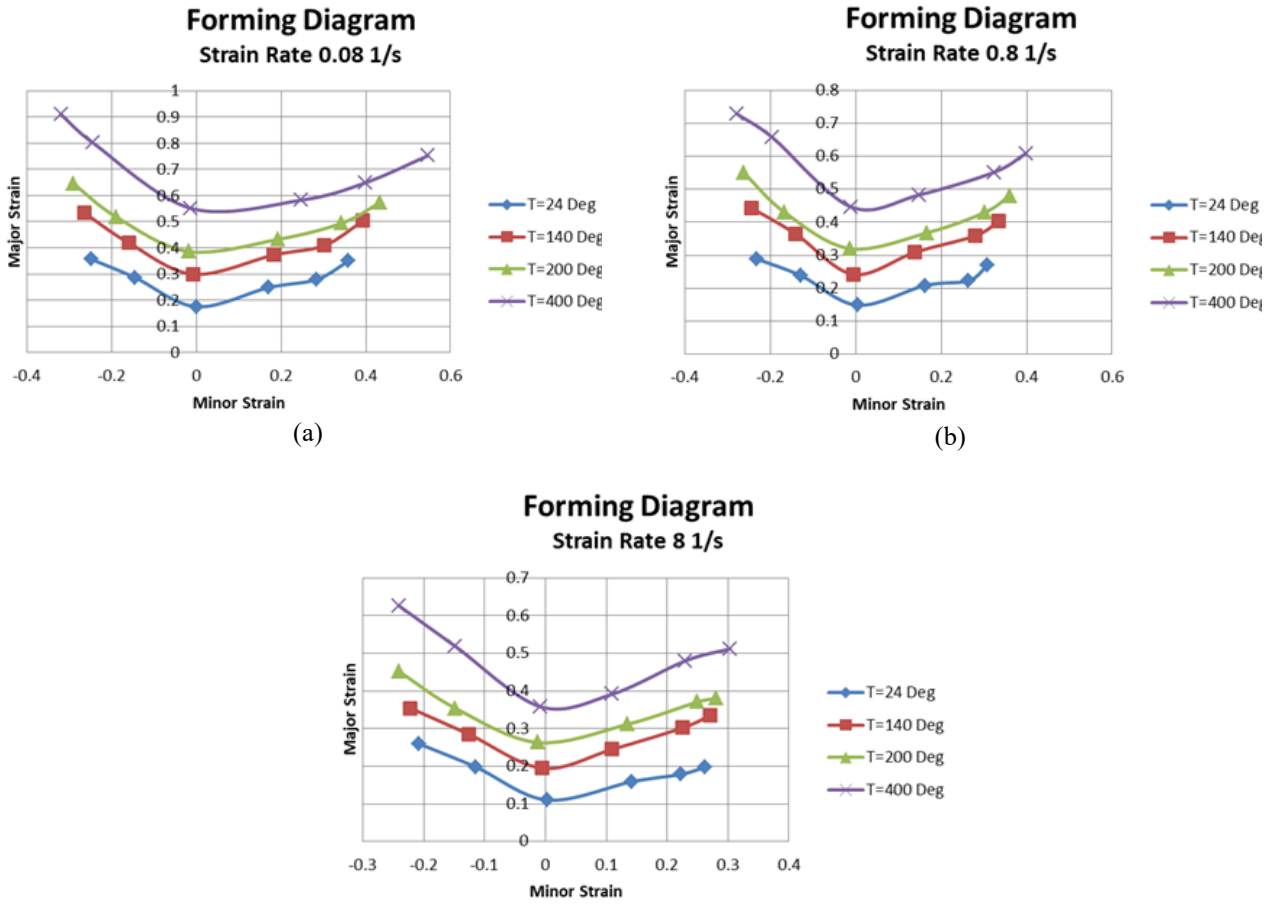

Figure 13. Comparing the FLC for diverse aluminum 6061 widths and temperatures at constant strain rate.

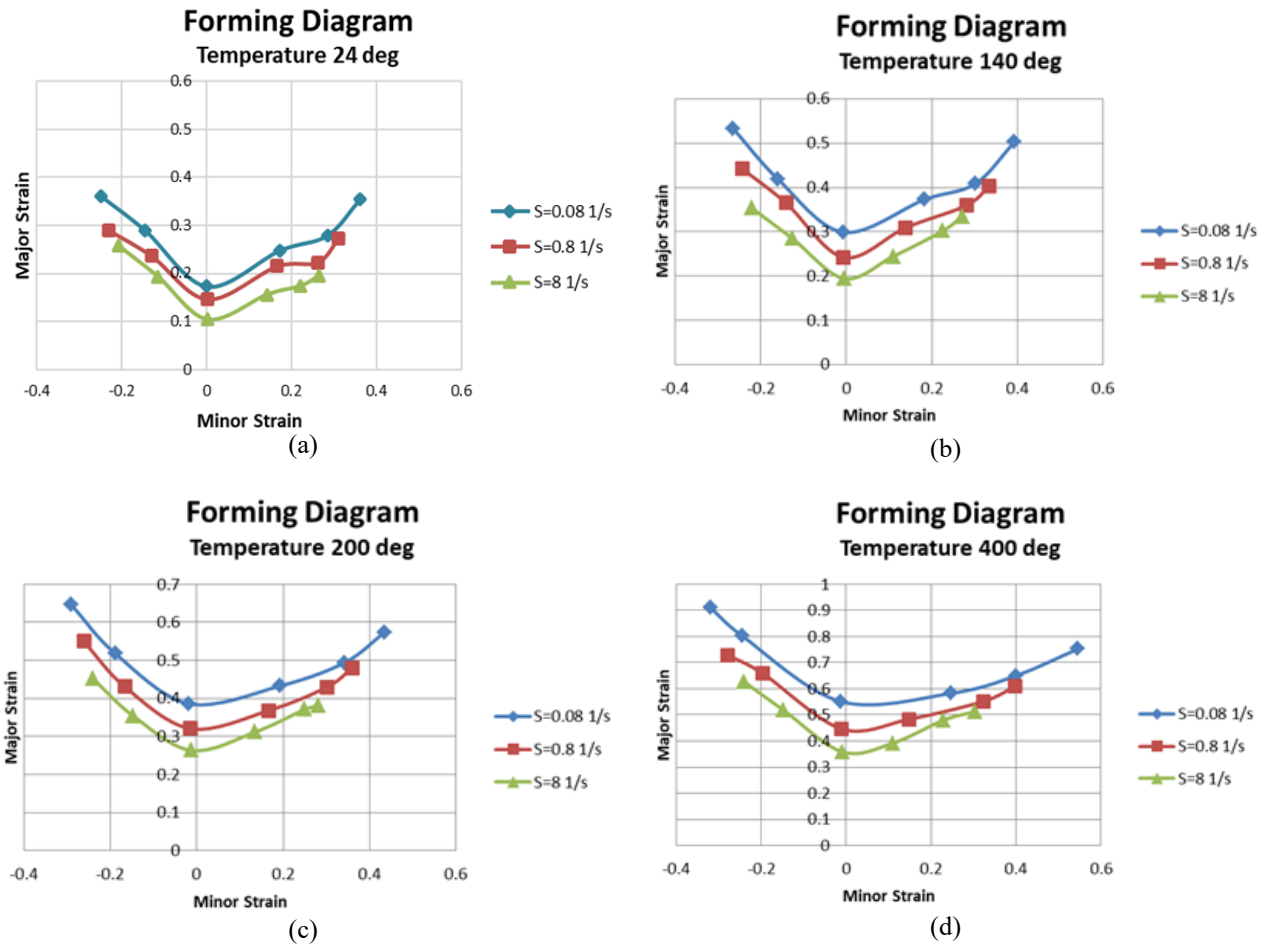

Figure 14. Comparison of FLC for different aluminum 6061 widths and strain rates at a constant temperature.

Figure 15 shows all the curves at various temperatures and strain rates. In the lowest case, it can be seen the forming limit curve at ambient temperature and high strain rate, and in the highest case, it can be observed the forming limit curve for the temperature of 400 degrees and the low strain rate. Some curves were achieved very close to each other, for example, for a temperature of 140 degrees with a strain rate of 0.08 per second and a temperature of 200 degrees with a strain rate of 0.8 per second, the curves were almost overlapped or a temperature of 140 degrees with a strain rate of 0.8 per second and a temperature of 200 degrees with a strain rate of 8 seconds. Stress distribution in aluminum foil is one of the important points. According to Figure 15, by increasing the width of the sheet, the stress values were reduced. As the process temperature raised, the strain values increased and the stress values decreased. Higher strain rates also resulted in lower stresses. In two-stage forming, the FLC was extracted in the same way as single-stage forming. Since this analysis was carried out for ambient temperature and strain rate of 0.08 per second, its forming limit curve was a curve illustrated in Figure 16. In this figure, this curve was compared with a single-stage limiting curve for the same temperature and strain rate. It was obvious that by creating the initial strain on the sheet in the first stage and then forming in the second stage, the forming limit curve was moved upwards and of course, the changes were greater for larger values.

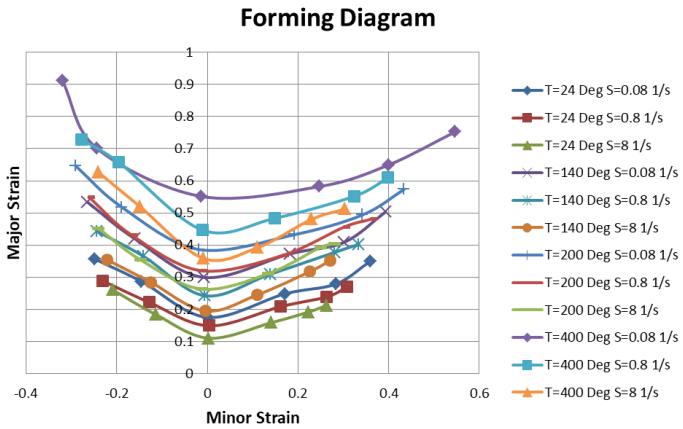

Figure 15. Comparison of FLC for different aluminum 6061 widths, temperatures, and strain rates.

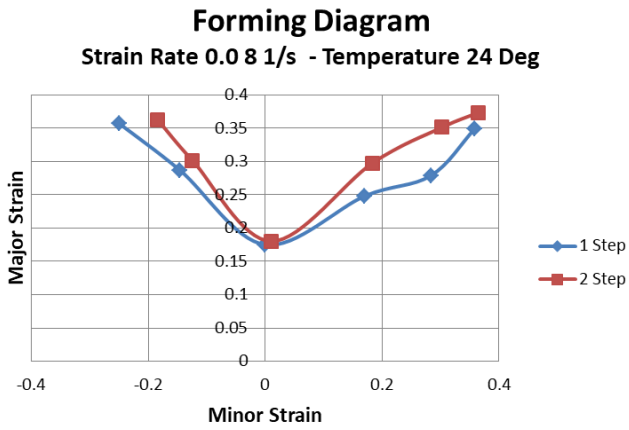

Figure 16. Comparison of one-stage and two-stage aluminum 6061 forming limit curve at 24°C and strain rate 0.08.

By performing data, analysis on the results obtained from single-stage analyzes, minor and major strain changes were determined separately under the effect of temperature for various sheet widths (Figure 17). For positive values of minor strain, by increasing temperature, the strain was also augmented with a slight slope. For its negative values, the strain was minimized with a slight slope and for its value close to zero, the changes were so small and the slope of the curve was close to zero. For major strain, in all latitudes, by raising the temperature, the strain also raised, and the slope of this augmentation was greater than the minor strain. It performs good formability at higher temperatures due to the fact that the elongation is the largest, and high ductility can postpone localized deformation, which benefits the formability. Then, by using data analysis, a two-stage forming limit curve for temperatures of 140°C, 200°C, and 400°C was predicted. This prediction was made using the slope of the changes of each of the minor and major strains for different widths. The results of this prediction are depicted in Figure 18. Therefore, several two-stage analyzes were performed to validate the results, which are shown as scattered points in this diagram. Comparison of forecast results with finite element analysis represented errors of less than 8% (Table 5). Von Mises stress distribution for one and two-stage forming of aluminum 6061 sheets are shown in Figures 19 and 20.

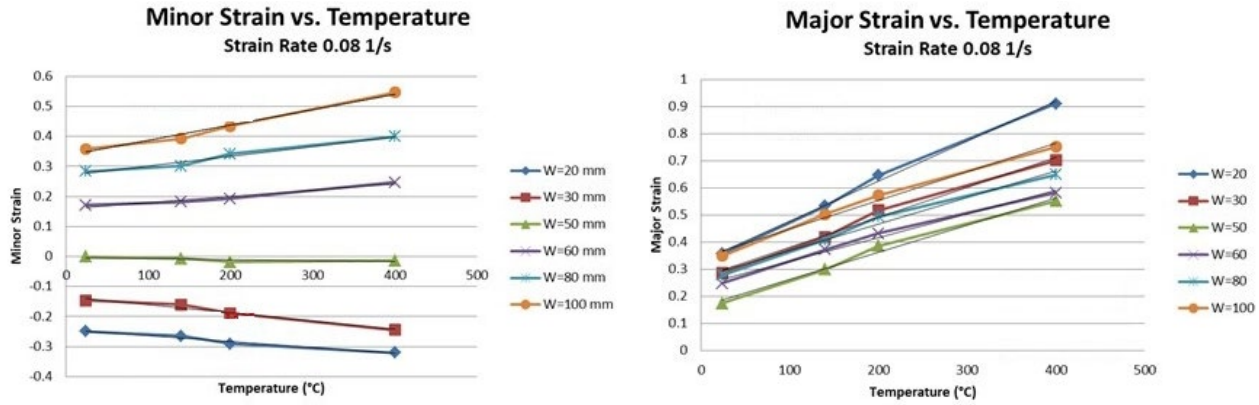

(a) (b)

Figure 17. Changes of (a) minor and (b) major strain relative to temperature for aluminum 6061 sheet tensile at a strain rate of 0.08 per second.

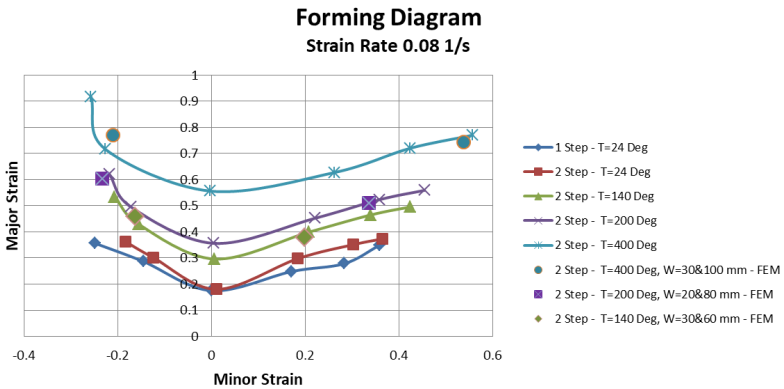

Figure 18. Comparison of the two-stage forming limit curve predicted at different temperatures with the values of finite element model.

Table 5. The error of predicted values relative to finite element analysis in forming two stages with different temperatures.

Major strain error (%)	Minor strain error (%)	Temperature (°C)	Width (mm)
3.3	3.5	400	100
7.4	7.8	400	30
2.7	6.5	200	80
3.1	6.2	200	20
5	4.7	140	60
6.7	4.2	140	30

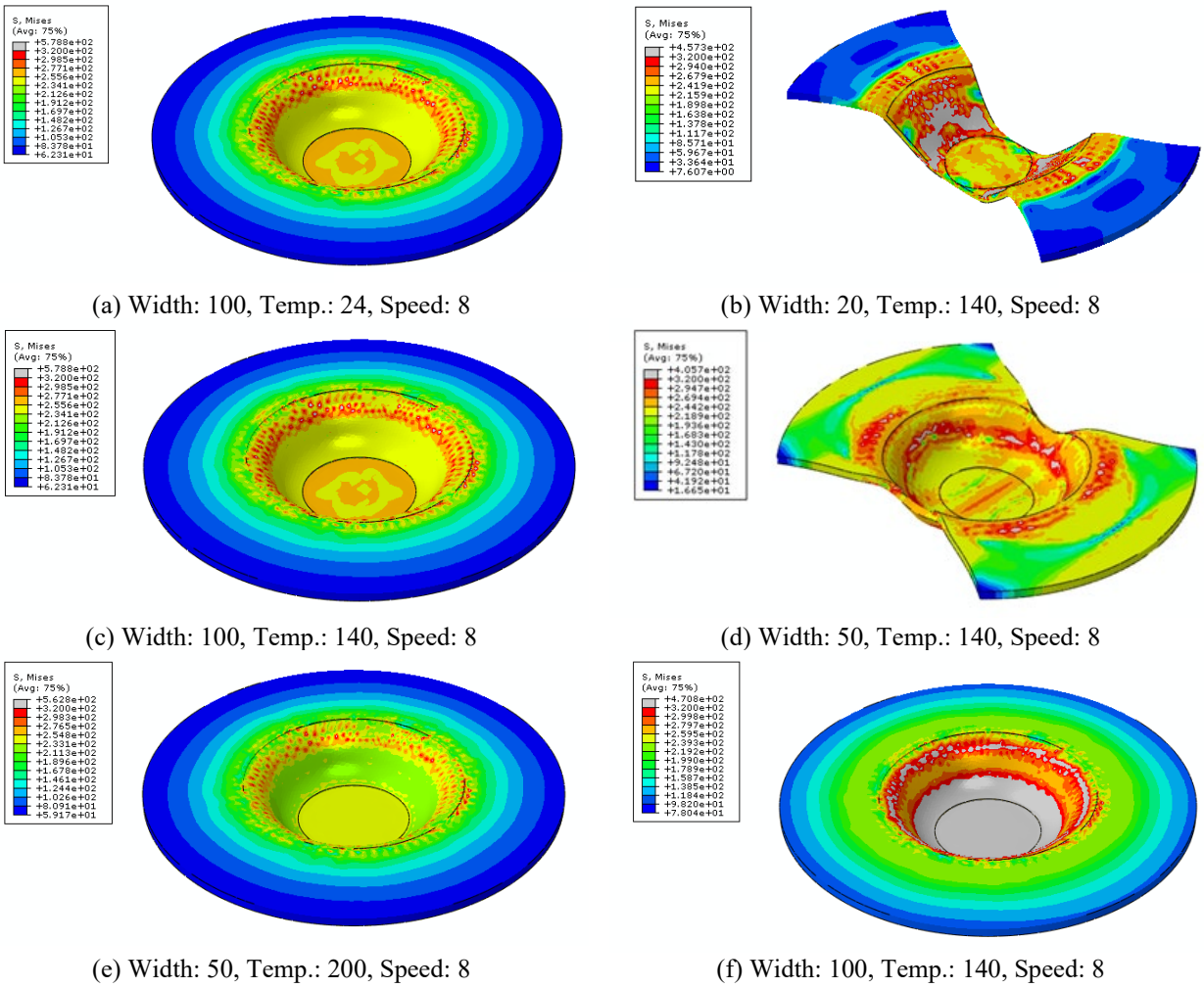

(a) Width: 100, Temp.: 24, Speed: 8

(b) Width: 20, Temp.: 140, Speed: 8

(c) Width: 100, Temp.: 140, Speed: 8

(d) Width: 50, Temp.: 140, Speed: 8

(e) Width: 50, Temp.: 200, Speed: 8

(f) Width: 100, Temp.: 140, Speed: 8

Figure 19. Von Mises stress distribution for forming one-stage aluminum 6061 in several samples of analyzes performed (MPa).

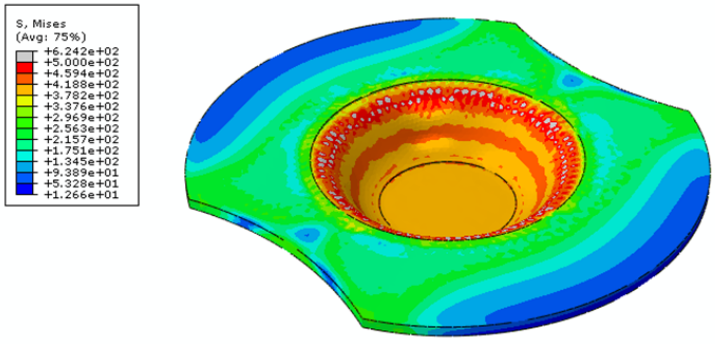

Figure 20. Von Mises stress distribution for two-stage aluminum 6061 forming with 80 mm width, 24°C temperature, and 0.08 strain rate.

CONCLUSION

The Form Limit Curve (FLC) is a significant concept for define sheet metal ductility. The ductility of the aluminum 6061 alloy sheet was considered in the present research. Also, the variations in the forming curve of aluminum 6061, which is widely used in the automobile industry, were investigated. For various temperatures and strain rates, these curves were obtained and compared. The proposed Lin-Voce constitutive model is suitable to describe the forming behaviour of aluminum 6061 under different strain conditions. It was found that increasing the temperature led the curve to rise and fall, while raising the strain rate caused the curve to fall and contract. Furthermore, for two-stage forming, the forming limit curve was produced and projected at temperatures above ambient temperature when the initial strain was formed in the sheet in the first stage, and the anticipated strain error was acceptable when compared to the finite element model. As a result, it was revealed that by having the FLC at one temperature, it is able to predict the two-stage forming limit curve at two temperatures. The formability at high punch speed was always lower than that at low punch speed at a given temperature, demonstrating that strain rate had a detrimental impact on sheet formability.

REFERENCES

[1] S. David, L. Jeff, and G. John, *Fundamentals of tool design. American society of tool and manufacturing engineers*. New Delhi: Prentice-Hall, 2003.

[2] S.P. Rudraksha, and S.H. Gawande, "Effect of process parameters on coefficient of friction in tube hydroforming," *J. Bio-and Tribo-Corr.,* vol.7, no. 1, pp. 1-9, 2021.

[3] P.S. Raj, and A.C. Reddy, "Optimization of process parameters in deep drawing of monel-400 conical cup," *Int. J. Mech. Eng.*, vol. 10, no. 1, pp. 11-20, 2021.

[4] G. Devendar, and A.C. Reddy, "Parametric optimization of monel 400 cold deep drawn cylindrical cups," *Int. J. Mat. Sci.,* vol. 16, no. 1, pp. 17-31, 2021.

[5] M.J. Krishna, and A.C. Reddy, "Evaluation of process parameters of conical cups in incremental deep drawing process," *Int. J. Sci. Res*., vol. 7, no. 6, pp. 1345-1350, 2018.

[6] A. Kacem, H. Laurent, and S. Thuillier, "Experimental and numerical investigation of ductile fracture for AA6061-T6 sheets at room and elevated temperatures," *Int. J. Mech. Sci.,* vol. 222, no. 107201, 2022, doi: 10.1016/j.ijmecsci.2022.107201.

[7] S.P. Keeler, "Plastic instability and fracture in sheets stretched over rigid punches," Doctoral dissertation, Massachusetts Institute of Technology, USA, 1961.

[8] G.M. Goodwin, "Application of strain analysis to sheet metal forming problems in the press shop," *Sae Trans.,* 1968, vol. 1, pp. 380-387, 1968.

[9] R. Narayanasamy, and C.S. Narayanan, "Forming, fracture and wrinkling limit diagram for if steel sheets of different thickness," *Mater. Des.,* vol. 29, no. 7, pp. 1467-1475, 2008, doi: 10.1016/j.matdes.2006.09.017.

[10] S. Ahmadi, A.R. Eivani, and A. Akbarzadeh, "Experimental and analytical studies on the prediction of forming limit diagrams," *Com. Mater. Sci.,* vol. 44, no. 4, pp. 1252-1257, 2009, doi: 10.1016/j.commatsci.2008.08.008.

[11] T. Naka, G. Torikai, R. Hino, and F. Yoshida, "The effects of temperature and forming speed on the forming limit diagram for type 5083 aluminum–magnesium alloy sheet," *J. Mater. Process Tech.,* vol. 113, no. 1-3, pp. 648-653, 2001, doi: 10.1016/S0924-0136(01)00650-1.

[12] A.F. Graf, and W.F. Hosford, "Calculations of forming limit," *Metall Trans. A*., vol. 24, no. 11, pp. 2497-2501, 1993.

[13] T. Matsuoka, and C. Sudo, Effect of strain path on the fracture strain of steel sheet," *SUMITOMO search,* vol. 1, 71-80, 1969.

[14] K. Bandyopadhyay, S. Basak, S.K. Panda, and P. Saha, "Use of stress based forming limit diagram to predict formability in two-stage forming of tailor welded blanks," *Mat. Des.* 67: 558-570, 2015, doi: 10.1016/j.matdes.2014.10.089.

[15] R. Hill, "A theory of the yielding and plastic flow of anisotropic metals," *Proceedings of the Royal Society of London. Series A. Math. Phys. Sci.,* vol. 193, no. 1033, pp. 281-297, 1948.

[16] H.J. Bunge, K. Pöhlandt, and A.E. Tekkaya, *Formability of metallic materials: plastic anisotropy, formability testing, forming limits*. Heidelberg, Germany: Springer Science & Business Media, 2000.

[17] S.J. Hashemi, F. Rahmani, and S.M.H. Seyedkashi, "Numerical and experimental investigation of forming limit diagram in warm incremental forming process of aluminum tubes," *Modares Mech. Eng.,* vol. 20, no. 6, pp. 1635-1645, 2020.

[18] F. Rahmani, S.M.H. Seyedkashi, and S.J. Hashemi, "Experimental study on warm incremental tube forming of aa6063 aluminum tubes," *Int. J. Eng.,* vol. 33, no. 9, pp. 1773-1779, 2020, doi: 10.5829/ije.2020.33.09c.11.

[19] R. Saxena, R.G. Narayanan, and P.S. Robi, "Performance evaluation of stamping lubricants during elevated temperature forming of SS304 sheets using forming limit diagram," *Mat. Today: Proc.,* vol. 44, pp. 1761-1764, 2021.

[20] Z. Li, G. Zhou *et al.*, "Forming limits of magnesium alloy AZ31B sheet at elevated temperatures," *Int. J. Plastic,* vol. 135, no. 102822, 2020, doi: 10.1016/j.ijplas.2020.102822.

[21] C. Zhang *et al.*, "Effects of temperature and strain rate on the forming limit curves of AA5086 sheet," *Procedia Eng*., vol. 81, pp. 772-778, 2014, doi: 10.1016/j.proeng.2014.10.075.

[22] X. Chu, L. Leotoing, D. Guines, and E. Ragneau, "Temperature and strain rate influence on AA5086 forming limit curves: Experimental results and discussion on the validity of the MK model," *Int. J. Mech. Sci.,* vol. 78, pp. 27-34, 2014, doi: 10.1016/j.ijmecsci.2013.11.002.

[23] N. Maat, M.K.M. Nor, and C.S. Ho, "Characterization of mechanical properties, damage progression and fracture modes of recycled aluminium alloys AA6061 reinforced alumina oxide," *Int. J. Integrated Eng.,* vol. 13, no. 7, pp. 215-225, 2021.

[24] X. Fan, T. Suo, Q. Sun, and T. Wang, "Dynamic mechanical behavior of 6061 al alloy at elevated temperatures and different strain rates," *Acta Mech. Solida Sin.,* vol. 26, no. 2, pp. 111-120, 2013, doi: 10.1016/S0894-9166(13)60011-7.

[25] K.G. Hoge, "Influence of strain rate on mechanical properties of 6061-T6 aluminum under uniaxial and biaxial states of stress," *Exp. Mech.,* vol. 6, no. 4, pp. 204-211, 1966, doi: 10.1007/BF02326150.

[26] S. Mahabunphachai, and M. Koç, "Investigations on forming of aluminum 5052 and 6061 sheet alloys at warm temperatures," *Mat. Des.,* vol. 31, no. 5, pp. 2422-2434, 2010, doi: 10.1016/j.matdes.2009.11.053.

[27] A. Gilat, J.D. Seidt, T.A. Matrka, and K.A. Gardner, "A new device for tensile and compressive testing at intermediate strain rates," *Exp. Mech.,* vol. 59, no. 5, pp. 725-731, 2019.
[28] C.H. Wei, Y.P. Guan, and Z.H. Wang, 2016 "Hot deformation behavior of high Ti 6061 Al alloy," *Trans. Nonfer. Met. Soc. China*, vol. 26, no. 2, pp. 369-377, 2016, doi: 10.1016/S1003-6326(16)64129-8.
[29] Z. Chen, G. Fang, and J.Q. Zhao, "Formability evaluation of aluminum alloy 6061-T6 sheet at room and elevated temperatures," *J. Mat. Eng. Perf*. vol. 26, no. 9, pp. 4626-4637, 2017, doi: 10.1007/s11665-017-2895-0.
[30] R. Safdarian, Stress based forming limit diagram for formability characterization of 6061 aluminum," *Trans. Nonfer. Met. Soc. China*, vol. 26, no. 9, pp. 2433-2441, 2016, doi: 10.1016/S1003-6326(16)64350-9.